Surface core-level shifts on Ge(111)$c(2 \times 8)$: Experiment and theory

M. Kuzmin,[1,2,*] M. J. P. Punkkinen,[1,3] P. Laukkanen,[1,4] J. J. K. Lång,[1] J. Dahl,[1] V. Tuominen,[1] M. Tuominen,[1] R. E. Perälä,[1] T. Balasubramanian,[5] J. Adell,[5] B. Johansson,[3,6] L. Vitos,[3,6,7] K. Kokko,[1] and I. J. Väyrynen[1]

[1]*Department of Physics and Astronomy, University of Turku, FIN-20014 Turku, Finland*
[2]*Ioffe Physical-Technical Institute, Russian Academy of Sciences, St. Petersburg 194021, Russian Federation*
[3]*Applied Materials Physics, Department of Materials Science and Engineering, Royal Institute of Technology, SE-10044 Stockholm, Sweden*
[4]*Optoelectronics Research Centre, Tampere University of Technology, FIN-33101 Tampere, Finland*
[5]*MAX-lab, Lund University, SE-221 00 Lund, Sweden*
[6]*Condensed Matter Theory Group, Physics Department, Uppsala University, SE-75121Uppsala, Sweden*
[7]*Research Institute for Solid State Physics and Optics, P. O. Box 49, H-1525 Budapest, Hungary*

(Received 28 March 2011; published 28 June 2011)

Combining high-resolution photoelectron spectroscopy and density functional theory (DFT) calculations, 3*d* photoemission line shape and surface core-level shifts have been reinvestigated on the Ge(111)$c(2 \times 8)$ surface. It is found that 3*d* spectra include, in addition to the bulk and three surface-shifted components reported in literature, a component that was not identified in earlier measurements with a lower resolution. The detailed interpretation of these spectra and their line shape is made on the basis of DFT calculations. It is shown that the lowest binding energy component is due to the rest atoms. The higher binding energy emission is caused by the adatoms and the third-layer atoms that are below the adatoms. Finally, the two other surface components originate from the first- and second-layer atoms. The screening effects in the Ge(111)$c(2 \times 8)$ are discussed.

DOI: 10.1103/PhysRevB.83.245319 PACS number(s): 79.60.Bm, 71.15.Mb, 68.47.Fg

I. INTRODUCTION

Despite the detailed understanding of atomic and electronic structure of Ge(111)$c(2 \times 8)$ (Refs. 1–3 and reference therein), the number and atomic origins of surface-shifted components in core-level spectra from this reconstruction have still remained an open issue. In earlier studies, 3*d* photoemission was deconvoluted with the bulk (B) and two surface-related (S_1 and S_2) spin-orbit doublets.[4–11] The surface core-level shift (SCLS) of S_1 was identified between -0.27 and -0.23 eV relative to the bulk, and that of S_2 was found in the range of -0.8 to -0.72 eV. As the latter component is strongly shifted toward the lower binding energy and significantly separated from the other components, the presence of S_2 was justified. Its interpretation, however, was controversial. The S_2 was assigned to the adatoms[9–11] and the rest atoms[6,8] in the $c(2 \times 8)$ reconstruction. The S_1 was interpreted as originating from the "remaining" surface atoms, i.e., the first-layer atoms together with the rest atoms[9] or adatoms (Refs. 6 and 8). All those measurements were performed with the total energy resolution of 0.2–0.3 eV, and, therefore, a more detailed analysis of the 3*d* line shape was complicated.

Later, a third surface component (S_3) was resolved in 3*d* spectra taken with a higher resolution (80–90 meV).[12] The SCLS of S_3 is 0.17 eV, i.e., it is shifted to the higher binding energy. The atomic origin of this component was assumed to be the adatoms, while the S_1 and S_2 were assigned to the first-layer atoms and half the rest atoms, respectively. The assignment of S_2 in Ref. 12 was based on two facts. First, there are two inequivalent rest atoms in the $c(2 \times 8)$ unit cell, which can lead to a binding-energy split for such atoms. Second, the intensity of S_2 was about half of the intensity of the component related to the adatoms (S_3), whereas the total number of rest atoms is equal to the number of adatoms in the $c(2 \times 8)$ structure. The presence of S_1, S_2, and S_3 for the Ge(111)$c(2 \times 8)$ has also been confirmed independently.[13,14] However, no theoretical core-level investigation has been so far reported for this surface. Using a*b initio* molecular-dynamics calculations, it was found that there are some distortions in the first, second, and third layers of Ge(111)$c(2 \times 8)$.[2] Therefore, the number of bonding sites in this reconstruction is rather large, and it differs from the number of hitherto measured SCLSs. Thus, core-level measurements with an improved resolution combined with *ab initio* SCLS calculations are required to clarify the Ge 3*d* line shape.

In this study, we have combined high-resolution photoelectron spectroscopy using the synchrotron radiation and density functional theory (DFT) calculations to reinvestigate SCLSs on Ge(111)$c(2 \times 8)$ both experimentally and theoretically. The paper is organized as follows. The experimental and calculational details are given in Sec. II. The measured 3*d* spectra and identified SCLSs are presented and discussed in Secs. III A and III B. DFT SCLSs calculated for the optimized atomic structure of Ge(111)$c(2 \times 8)$ are shown and compared with measured data in Secs. III C and III D. Finally, the screening effects in the Ge(111)$c(2 \times 8)$ reconstruction are discussed in Sec. III E.

II. EXPERIMENTAL AND CALCULATIONAL DETAILS

The measurements were carried out at the MAX-lab synchrotron radiation facility (beamline I4, MAX-III) in Lund, Sweden. The Ge samples were cut from an Sb-doped (n-type) (111) wafer. Sample cleaning was performed by repeated cycles of Ar ion sputtering ($E = 0.7-1.0$ keV, $T = 775$ K) and subsequent annealing (900 K) until a sharp $c(2 \times 8)$ low-energy electron diffraction pattern was observed at 300 and 100 K. Sample heating was performed by direct current. The photoelectron spectra were acquired at 100 K by using the SPECS Phoibos 100 analyzer. The acceptance angle of electrons was $\pm 8^\circ$. The measured total energy resolution, defined by the analyzer, photon beam, and sample temperature broadening, was 48, 52, 55, and 58 meV at the photon energy $h\nu = 40$, 55, 70, and 90 eV, respectively. The binding energy

 ©2011 American Physical Society

is referred to the Fermi-level energy of a reference Ta sample in a good contact with the Ge sample.

The calculations were performed by using Vienna *ab initio* simulation package (VASP),[15] applying the projector augmented wave (PAW) method[16] and the local density approximation (LDA) of Ceperley and Alder,[17] as parametrized by Perdew and Zunger.[18] The optimization of the atomic structure was carried out utilizing conjugate-gradient minimization of the total energy with respect to the atomic coordinates. The Ge 3*d* electrons were treated as core electrons. The inclusion of the 3*d* electrons as valence electrons was tested as well. The results were very similar, i.e., the difference in SCLS did not exceed a few millielectron volts within the two treatments. The SCLS values were evaluated by using the average electrostatic potential at the core of the Ge atoms,[19] which was obtained by placing a test charge with the norm 1 at each Ge ion. The bulk reference value was obtained by averaging from layers 5–8. In the complete screening calculations a single core electron was excited from the core to the valence by generating the corresponding core-excited PAW potential,[20] and only the screening by valence electrons was thus included.

III. RESULTS AND DISCUSSION

A. 3*d* spectra

Figure 1 shows a series of raw 3*d* spectra taken at various photon energies ($h\nu = 40$, 55, 70, and 90 eV) and emission angles ($\theta_e = 0°$, 60°, and 80°). Each spectrum is normalized to its maximum. Even without any fitting it is evident that the spectra include at least four components labeled B, S_1, S_2, and S_3. The binding energy of the bulk component, B, can roughly be deduced from the most bulk-sensitive spectrum at $h\nu = 40$ eV and $\theta_e = 0°$ (the top curve in Fig. 1). It shows a pronounced peak at the binding energy of ~29.4 eV, which is strongly contributed by the bulk $3d_{5/2}$ emission. This peak clearly has a shoulder at ~29.1 eV of which intensity increases with changing the photon energy from 40 to 90 eV (i.e., with increasing the surface sensitivity). Therefore, the spectra include at least one surface-shifted emission near this binding energy (the component S_1 in Fig. 1). A well-resolved feature at ~28.6 eV is due to a component S_2 with the lowest binding energy. Finally, the spectra at $h\nu = 90$ eV indicate a complicated structure at ~29.7 eV. The intensity of this feature depends on the emission angle, and this behavior cannot be explained by variation in intensity of B, S_1, and S_2. Hence, a fourth component (S_3) at the higher binding energy can be assumed.

It is also seen in Fig. 1 that the spectra are influenced by $h\nu$ and θ_e not systematically. In particular, the most bulk-sensitive spectrum at $h\nu = 40$ eV and $\theta_e = 0°$ (the kinetic energy of electrons is 4–8 eV) reveals, in addition to the bulk emission, a relatively large contribution from the surface atoms. Moreover, the intensity of S_2 is strongly affected by θ_e at $h\nu = 70$ eV, but it is not at $h\nu = 55$ and 90 eV. In contrast, the S_1 is affected by θ_e at $h\nu = 55$ but not at $h\nu = 70$ and 90 eV. Thus, we propose that the nonsystematic variation of 3*d* line shape is due to the diffraction effects, in agreement with Refs. 8 and 11. Therefore, the intensity ratios of B, S_1, S_2, and S_3 might not straightforwardly reflect the number ratios of respective atoms.

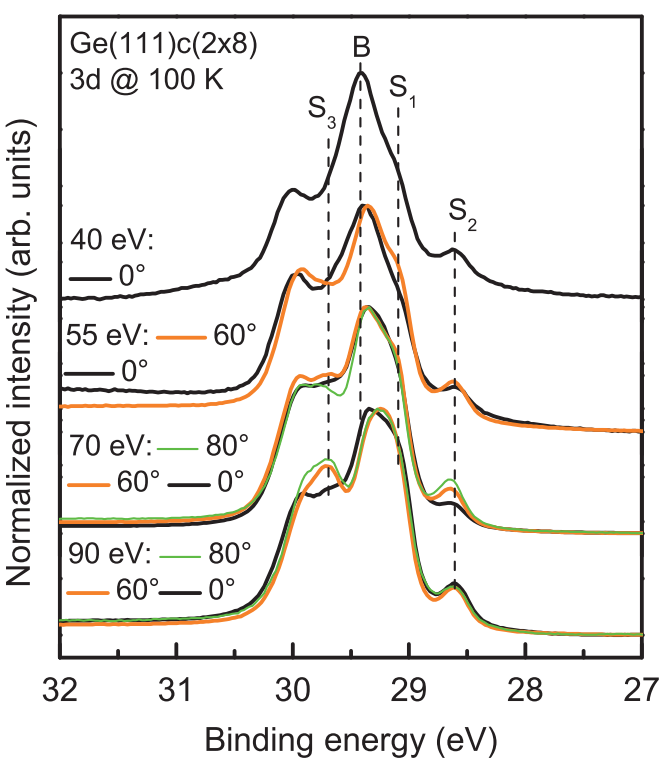

FIG. 1. (Color online) Normalized 3*d* spectra of Ge(111)$c(2 \times 8)$ taken with different photon energies and emission angles at 100 K. The obvious spectral components (B, S_1, S_2, and S_3) are indicated by dash lines (see the text for more detailed explanation).

B. Measured SCLSs

A more detailed analysis of the 3*d* spectra was done by using a standard least-squares fitting procedure with a linear combination of spin-orbit-split Voigt functions. The background was removed by the Shirley method. In the beginning, the fitting scheme with four components (B, S_1, S_2, and S_3) was tested. It is similar to the fitting scheme in Refs. 12–14. The Lorentzian full width at half maximum (LW) and spin-orbit splitting (SOS) were kept constant for all the components when fitting the whole series of spectra at different $h\nu$ and θ_e. The LW was always fixed at 0.150 eV. The SOS was chosen in the range of 0.570–0.595 eV, and different values were tested out. Then, the optimized SOS was fixed as well. In earlier studies, the SOS was typically 0.580–0.586 eV,[4,5,7,8,10,13,14,21–23] although other values were also reported (e.g., 0.550 eV in Ref. 6 and 0.590 eV in Ref. 9). The branching ratio (BR) was assumed to vary slightly (±10%) for different components around 0.667 (2:3) because of the diffraction effects. In previous studies, the BR was typically 0.58–0.68 for the Ge(111)$c(2 \times 8)$ surface,[4–7,12–14,21–23] and it was recently found between 0.649 and 0.707 for the Ge(001)$c(4 \times 2)$ (Ref. 24). It was also taken into account that the BR was 0.640 for Sb/Ge(111)(2×1)[25,26] and 0.625 for Bi/Ge(111)$(\sqrt{3} \times \sqrt{3})R30°$ (Ref. 26), and the SOS was 0.580 eV for both. In these reconstructions, the Ge substrate structure is brought into the bulklike configuration by the group-V adsorbates, leading to a single spin-orbit doublet in Ge 3*d* spectra. Thus, the Ge 3*d* fitting parameters can be easily

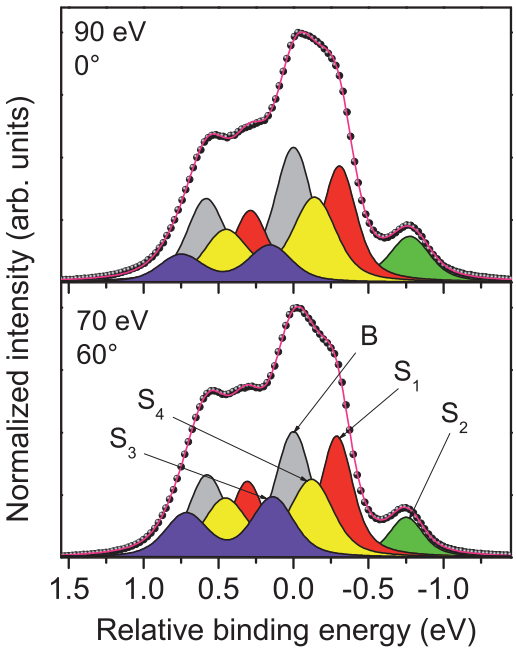

FIG. 2. (Color online) Decomposition of 3d spectra at $(h\nu, \theta_e) =$ (70 eV, 60°) and (90 eV, 0°). The measured data are filled dots. The shadowed doublets are the bulk (B) and surface (S_1–S_4) components. The resultant fitting curve is shown by solid line. The relative binding energy is referred to the binding energy of B.

found for such systems. The Gaussian widths (GW), binding energies, and intensities of the components were allowed to vary in the present study.

Within the above fitting scheme, some individual 3d spectra could be successfully reproduced by the bulk and three surface components. However, keeping SCLSs unchanged for the whole series of spectra, i.e., at various $h\nu$ and θ_e, was definitely impossible (especially for S_2 and S_3). Therefore, we discard the fitting scheme with the bulk and three surface components.

An improved fit was obtained by introducing a fourth surface component S_4. This allowed us to avoid the above variation in SCLS. Moreover, reasonable GW values were obtained. In Fig. 2, fitting results are demonstrated for two spectra at ($h\nu = 70$ eV, $\theta_e = 60°$) and ($h\nu = 90$ eV, $\theta_e = 0°$). At these experimental conditions the fittings were most challenging, which most likely is due to the lack of a valley between the main peak and the higher binding-energy structure in these spectra. The dots represent the measured data and the solid lines the fitting curves. The bulk and four surface components are shown by shadowed doublets. The SCLSs of S_1, S_2, S_3, and S_4 are −0.290, −0.755, 0.150, and −0.125 eV, respectively. The GW of B is 0.198 eV at $h\nu = 70$ eV and 0.208 eV at $h\nu = 90$ eV. The GWs of S_1, S_2, S_3, and S_4 are, respectively, 0.194 [0.205], 0.161 [0.163], 0.239 [0.242], and 0.245 eV [0.250 eV] at $h\nu = 70$ eV [90 eV]. At the first glance, it is surprising that the GW of bulk emission is rather large as compared to that of S_2. This behavior will be rationalized below. We will show that the B is contributed by some surface atoms with experimentally unresolved core-level shifts, and thus the multiatomic origin of B leads to the increased GW. The optimized SOS is 0.588 eV. The quality of fittings was poorer with SOS of 0.57–0.58 eV. The BR was not constrained strictly,

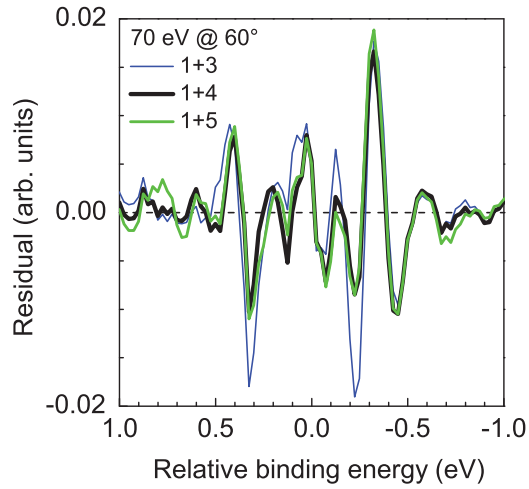

FIG. 3. (Color online) Residuals for the 3d spectrum at $h\nu =$ 70 eV and $\theta_e = 60°$. The curves are obtained within the fitting schemes with the bulk and three, four, or five surface components ("1+3", "1+4", and "1+5", respectively).

i.e., it was allowed to vary within 0.667±10%. Nevertheless, the average BR was found to be 0.658 at $\theta_e = 0°$ and 0.663 at $\theta_e = 60°$. These values agree quite well with the theoretical BR for the spin-orbit $d_{3/2-5/2}$ core emission (2:3).

Introducing additional surface components did not lead to the improvement of the fit. Figure 3 shows residuals obtained for the (70 eV, 60°) spectrum fitted with the bulk and three, four, or five surface components (the fitting schemes "1+3", "1+4", and "1+5", respectively). The thinnest line represents the residual for the fitting scheme "1+3". The thickest line gives the residual for the fitting scheme "1+4". It is seen that introducing S_4 improves the fit near the binding energies of −0.2 eV and 0.35 eV. This means that the component S_1 alone is not enough to reproduce the shoulder on the lower binding energy side of the main peak and that the S_4 is hidden in this energy region. On the other hand, the fitting with five surface components ("1+5") did not give any improvement, as seen in Fig. 3. Thus, we propose the fitting scheme "1+4" with four SCLSs, −0.290, −0.755, 0.150, and −0.125 eV for the 3d spectra of Ge(111)$c(2 \times 8)$ in Fig. 1. The S_4 (−0.125 eV) was not resolved in earlier studies where the resolution was lower than in the present work. The first two SCLSs, S_1 and S_2, were identified with the resolution of 0.2–0.3 eV,[4–11] whereas the third one, S_3, was found with the resolution of 80–90 meV (Ref. 12).

C. Atomic structure and calculated SCLSs

Although the favorable site for the adatoms in the Ge(111)$c(2 \times 8)$ is T_4,[1] we consider here two atomic configurations where the adatoms occupy either T_4 or H_3. These configurations are called T_4 and H_3 structures hereafter. The optimization of these structures was performed by VASP using the full-periodicity $c(2 \times 8)$ slab. It consisted of 10 single atomic layers (i.e., 5 double layers), one-fourth monolayer (ML) of adatoms on one (111) surface of the slab (on top), and 1 ML of hydrogen atoms on the other (111) surface (at the bottom). In the fully relaxed atomic geometry, the energy difference of T_4 and H_3 sites is found to be 0.08 eV/(1×1),

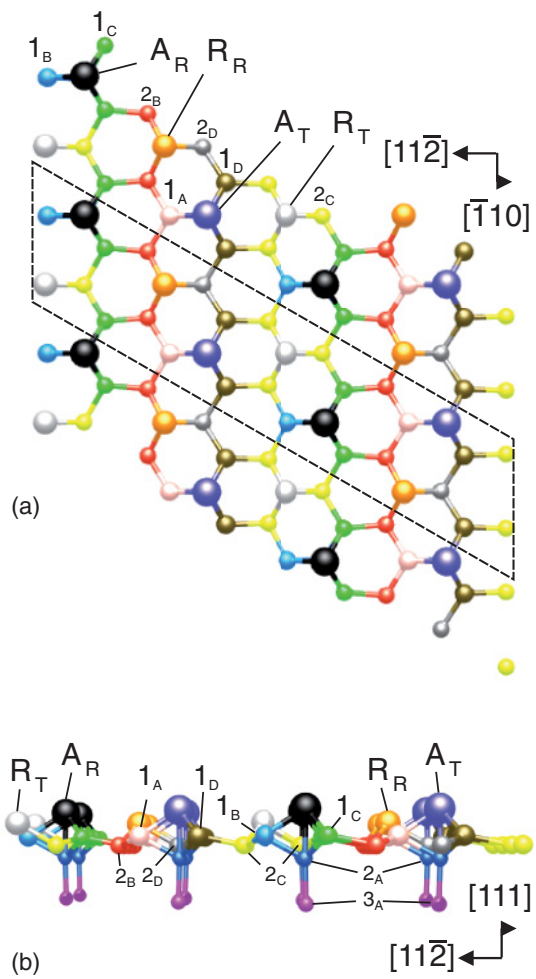

FIG. 4. (Color online) Atomic model of the T_4 structure of Ge(111)$c(2 \times 8)$. (a) Top view and (b) side view. The $c(2 \times 8)$ unit cell is outlined in (a). The atoms are labeled (see in the text for more details).

in good agreement with Ref. 2. The top and side views of the fully optimized T_4 structure are depicted in Fig. 4. The A_T and A_R adatoms are asymmetrically surrounded by three and four rest atoms, respectively. The R_T and R_R rest atoms are asymmetrically surrounded by three and four adatoms, respectively. These notations are taken from Ref. 3. The A_T is bonded to the first-layer atom 1_A and two atoms 1_D. The A_R is bonded to the atom 1_B and two atoms 1_C. The first-layer atoms are displaced from their ideal positions toward the adatoms. The R_T is bonded to three second-layer atoms 2_C and the R_R to the atom 2_D and two atoms 2_B. The adatoms can also interact with the second-layer atoms 2_A that are just below the adatoms and pushed downward with respect to 2_B, 2_C, and 2_D. This distortion in the second atomic layer is translated to the third layer, where the atom 3_A, which is located just below the atom 2_A (see the side view in Fig. 4), is significantly displaced downward from the ideal position. Thus, the $c(2 \times 8)$ reconstruction includes a number of different atoms: two adatoms, two rest atoms, four first-layer atoms, four second-layer atoms, and at least two third-layer atoms. The number of such atoms is much larger than the number of measured SCLSs.

TABLE I. Initial state (IS) and complete screening (CS) SCLSs calculated for different atoms in the T_4 structure. The atomic density is given in ML. One monolayer (1 ML) is referred to as the atomic density of the full single layer on the bulk-terminated Ge(111) [i.e., 16 atoms per c(2 × 8) unit cell]. The Δ_{SCLS} is defined as a difference of $SCLS_{CS}$ and $SCLS_{IS}$.

Type of atom	Atomic density (ML)	$SCLS_{IS}$ (eV)	$SCLS_{CS}$ (eV)	Δ_{SCLS} (eV)
		Adatoms		
A_T	1/8	0.100	−0.123	−0.223
A_R	1/8	0.101	−0.133	−0.234
		Rest atoms		
R_T	1/8	−0.619	−0.500	0.119
R_R	1/8	−0.601	−0.524	0.077
		First layer		
1_A	1/8	−0.231	−0.403	−0.172
1_B	1/8	−0.209	−0.371	−0.162
1_C	1/4	−0.191	−0.371	−0.18
1_D	1/4	−0.18	−0.362	−0.182
		Second layer		
2_A	1/4	−0.233	−0.418	−0.185
2_B	1/4	−0.178	−0.203	−0.025
2_C	3/8	−0.161	−0.209	−0.048
2_D	1/8	−0.121	−0.187	−0.066
		Third layer		
3_A	1/4	0.12	−0.092	−0.212
Third-layer				
atoms not		−0.065	−0.096	−0.031
shown in		−0.041	−0.103	−0.062
Fig. 4		−0.055	−0.112	−0.057
		−0.044	−0.087	−0.043

The buckling and in-plane asymmetry of rest atoms are, respectively, 0.040 and 0.130 Å in the T_4 structure and 0.086 and 0.149 Å in the H_3 structure. The buckling of adatoms is significantly smaller in the both structures (0.003 Å). The in-plane asymmetry of adatoms is 0.064 Å in the T_4 structure and 0.133 Å in the H_3 structure. Thus, the strain relief appears to be stronger in the T_4 structure, which is consistent with a higher stability of this configuration. In both T_4 and H_3 structures, the R_T atoms are raised above the first layer higher than the R_R atoms.

The SCLSs were calculated for both the T_4 and H_3 structures. The results are presented in Tables I and II. The difference in SCLS obtained in the complete screening model and the initial state model, $\Delta_{SCLS} = SCLS_{CS} - SCLS_{IS}$, is also shown for different atoms. Similar trends are observed for the two atomic structures. First, in addition to the adatoms, rest atoms, and first-layer atoms, some atoms in the second and third layers of the T_4 and H_3 structures produce significant core-level shifts, and, therefore, the measured spectra can be contributed by such atoms. The most negative SCLSs are found for the rest atoms. The binding-energy split of R_T and R_R is about 0.02 eV in the T_4 structure and 0.07–0.09 eV in the H_3 structure. Therefore, it is unlikely that the lowest

TABLE II. The same as Table I, but for the H3 structure.

Type of atom	Atomic density (ML)	$SCLS_{IS}$ (eV)	$SCLS_{CS}$ (eV)	Δ_{SCLS} (eV)
		Adatoms		
A_T	1/8	0.335	−0.12	−0.455
A_R	1/8	0.391	−0.05	−0.441
		Rest atoms		
R_T	1/8	−0.489	−0.488	0.001
R_R	1/8	−0.584	−0.561	0.023
		First layer		
First-layer atoms	3/8	−0.190	−0.455	−0.265
		−0.184	−0.392	−0.208
	3/8	−0.154	−0.405	−0.251
		−0.159	−0.372	−0.213
		Second layer		
Second-layer atoms	3/8	−0.285	−0.42	−0.135
		−0.278	−0.378	−0.1
	1/4	−0.254	−0.4	−0.146
	1/8	0.188	−0.02	−0.208
		Third layer		
Third-layer atoms	5/8	−0.109	−0.173	−0.064
		−0.107	−0.211	−0.104
		−0.096	−0.168	−0.072

binding-energy component S_2 is due to the half of the rest atoms (either R_T or R_R). For the adatoms, the SCLSs are positive within the initial state model. In the H_3 structure, the $SCLS_{IS}$ is 0.335 eV for the A_T and 0.391 eV for the A_R. In the T_4 structure, both the adatoms have the $SCLS_{IS}$ of ∼0.10 eV. In addition, the $SCLS_{IS}$ of the 3_A atom is 0.12 eV, which is the most positive shift in this structure. The $SCLS_{IS}$s of the other atoms are found between −0.233 and −0.041 eV in the T_4 structure and between −0.285 and 0.188 eV in the H_3 structure.

Within the complete screening model, $SCLS_{CS}$ values tend to move to the lower binding energy with respect to corresponding $SCLS_{IS}$ values for most surface atoms. The relaxation effect in the completely screened final state is not the same for different atoms, which can be seen from the analysis of Δ_{SCLS} values in Tables I and II. The most negative Δ_{SCLS} values are found for the adatoms in both the atomic structures, suggesting the most efficient complete screening after the core ionization of these atoms. In contrast, the $SCLS_{CS}$s of rest atoms are moved to the higher binding energy, and the Δ_{SCLS} values are positive for such atoms. We will discuss the screening effects in more detail below (Sec. III E).

D. Comparison of measured and calculated SCLS

It is obvious that differences in core-level binding energy for some surface atoms in Tables I and II (especially for the first- and second-layer atoms) are very small and cannot be resolved in the present study. Therefore, the number of SCLSs measured in Sec. III B differs from the number of calculated SCLSs in Sec. III C. The origin of the measured SCLSs can be interpreted

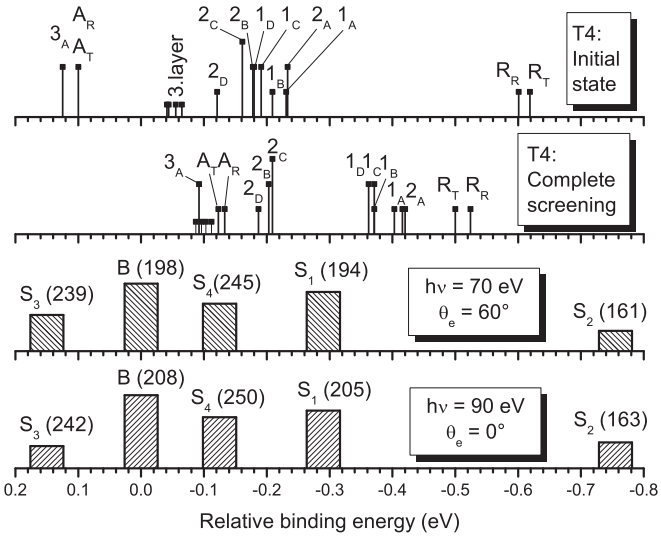

FIG. 5. Comparison of calculated and measured SCLSs. The calculated SCLS's are obtained for the T_4 structure within the initial state (IS) and complete screening (CS) model. The values in parenthesis represent the GW of components at $h\nu = 70$ and 90 eV. For other details see the text.

on the basis of calculated data. First, it is helpful to compare the energy range in which the measured SCLSs are observed with corresponding ranges of calculated $SCLS_{IS}$ and $SCLS_{CS}$ values for the T_4 and H_3 structures. The measured SCLS range is from −0.755 to 0.150 eV, as shown in Sec. III B. For the T_4 structure, the $SCLS_{IS}$ and $SCLS_{CS}$ ranges are from −0.619 to 0.12 eV and from −0.524 to −0.087 eV, respectively. For the H_3 structure, these ranges are from −0.584 to 0.391 eV and from −0.561 to −0.02 eV. The analysis shows that the S_3 component with the positive SCLS (0.15 eV) cannot be explained within the complete screening model, where all the surface atoms in the T_4 and H_3 structures are shifted to the lower binding energy. Within the initial state, the T_4 structure gives a more plausible explanation of 3*d* spectra than the H_3 structure. Moreover, the T_4 is energetically favorable over the H_3. Therefore, we interpret the atomic origin of measured 3*d* components on the basis of the T_4 structure.

Figure 5 compares the measured SCLSs (two bottom panels) and the calculated ones for the T_4 (two top panels). The positions of $SCLS_{IS}$ and $SCLS_{CS}$ values are shown by vertical bars. The height of bars is proportional to the numbers of respective atoms (Table I). The positions of measured SCLSs are shown by shadowed bars. The height of these bars is proportional to the intensity of respective components in the spectra of Fig. 2. The values in parenthesis give the GW's obtained in the fitting. The positive $SCLS_{IS}$s are found for the adatoms (0.10 eV) and the 3_A atom (0.12 eV). These shifts agree well with the SCLS of S_3, and, therefore, we assign this component to these atoms. Note that the S_3 was assigned to the adatoms in Ref. 12; however, the present study reveals that this component is additionally contributed by the 3_A atoms. The $SCLS_{CS}$s appear to be overestimated for the adatoms and the 3_A atom.

The lowest binding energy component S_2 (−0.755 eV) agrees better also with the T_4 structure. For this structure, the lowest binding-energy $SCLS_{IS}$ [$SCLS_{CS}$] is −0.619

[−0.500] eV for the rest atoms R_T and −0.601 [−0.524] eV for the R_R. For the H_3 structure, the lowest binding-energy $SCLS_{IS}$ [$SCLS_{CS}$] is −0.489 [−0.488] and −0.584 [−0.561] eV, respectively. Therefore, we interpret the S_2 as originating from both the R_T and R_R in the T_4 structure. The GW of S_2 is rather small (161–163 meV). This agrees with a small core-level binding-energy split of R_R and R_T (18 meV). Such interpretation is different from that of Ref. 12, where the S_2 was assigned to half the rest atoms. Note also that the GW of S_2 is significantly smaller than that of S_3 (239–242 meV) which is contributed by the adatoms and 3_A atoms. The total number of such atoms (four adatoms and four third-layer atoms) is twice as large as the number of rest atoms. The intensity ratio of respective S_3 and S_2 changes from 2 to 0.9 depending on the experimental condition, and hence, the intensity of these emissions is affected by the diffraction and attenuation effects, as discussed in Sec. III A.

It is worth noting that the $SCLS_{IS}$ data in Table I have a wide gap (0.368 eV), which is observed between the rest atoms and the 2_A atoms. This gap is consistent with the large binding energy difference between S_1 and S_2 in 3*d* spectra (0.465 eV) and explains a good separation of the S_2 emission from the other components (i.e., the lowest binding energy peak at 28.6 eV in the raw spectra of Fig. 1). The S_2 could be well resolved even with the 0.2- to 0.3-eV resolution (Refs. 4–11).

In contrast to S_2 and S_3, the interpretation of S_1 and S_4 is more ambiguous. As shown in Table I and Fig. 5, the first- and second-layer atoms cause eight $SCLS_{IS}$s ranging from −0.233 to −0.121 eV. Therefore, we assume that the S_1 (−0.29 eV) and S_4 (−0.125 eV) are contributed by these atoms. It is likely that the former component is largely due to the first layer and the latter to the second layer, although the atom 2_A can also contribute to S_1 and the atoms 1_C and 1_D to S_4.

The third-layer atoms, except for the 3_A, are slightly shifted to the lower binding energy (by 0.041–0.065 eV) from the bulk, and core emissions from these atoms are attenuated by the upper layers. Because it is unlikely that such emissions can be resolved in our measurements, we assume that the above third-layer atoms contribute to the *B* component, leading to the increased GW (198–208 meV). Thus, we argue that the 3*d* line shape in the energy region near the shoulder at ∼29.1 eV in Fig. 1 is caused by the emissions from the first- and second-layer atoms. The line shape near the main peak at 29.4 eV is due to the emissions from the bulk and third-layer atoms. In earlier studies, the S_4 was not resolved and the emission from the second and third layers was not considered at all.

E. Screening effect

Although the initial state theory accounts for the measured 3*d* spectra adequately (Sec. III D), it is important to consider the final-state data in more detail. Here, we analyze the Δ_{SCLS} in Tables I and II that illustrates the efficiency of complete screening for different atoms. In general, the final-state theory leads to an effect of shifting calculated initial state SCLSs to the lower binding energy. Note that we consider here the static (complete) relaxation of a core-ionized atom in the final state (i.e., the complete screening). This means that the redistribution of valence electron charge in response to the creation of core hole is assumed to occur faster than the emission of a photoelectron. In reality, however, the screening of core hole can be incomplete during the photoemission, and then the final-state theory can overestimate the above effect of shifting SCLS to the lower binding energy (e.g., Ref. 27). On the other hand, the initial state theory will underestimate the SCLS if the screening occurs fast enough. Thus, the $SCLS_{CS}$ and $SCLS_{IS}$ values appear to be the limits for the core-level shift of surface atoms. In addition, the complete screening theory suggests that the occupied and unoccupied density of states is sufficiently high for the screening process to take place.

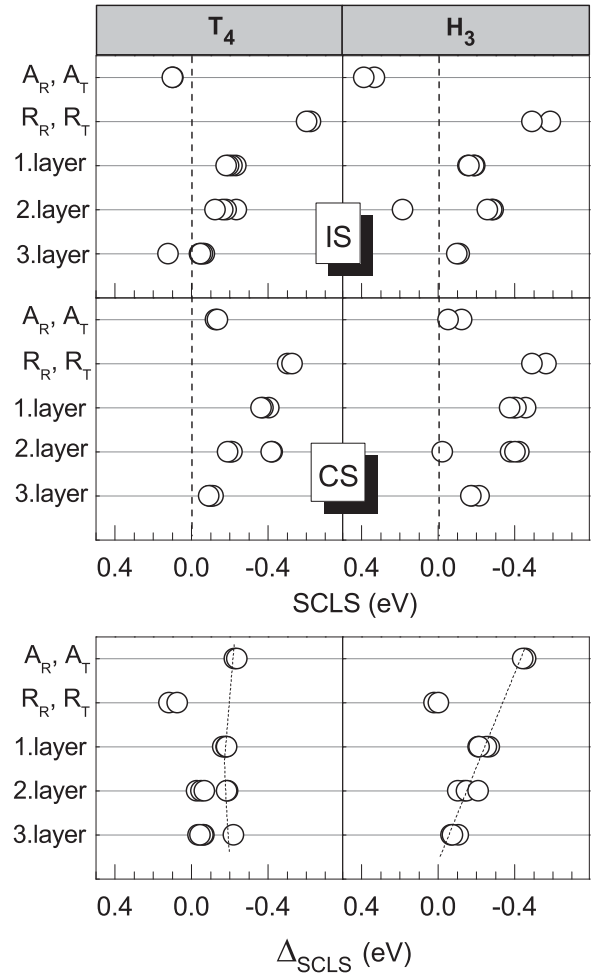

FIG. 6. Comparison of $SCLS_{IS}$, $SCLS_{CS}$, and Δ_{SCLS} values for the T_4 and H_3 structures.

The analysis of data in Tables I and II shows that in both T_4 and H_3 structures, most of $SCLS_{CS}$s are shifted to the lower binding energy relative to corresponding $SCLS_{IS}$s, that is, Δ_{SCLS}s are negative for such atoms. Figure 6 shows the distributions of $SCLS_{IS}$, $SCLS_{CS}$, and Δ_{SCLS} values for different atoms and layers in the T_4 and H_3 structures. It is seen that the adatoms have the most negative Δ_{SCLS} values in both structures, and, therefore, the screening is most efficient for these atoms. According to our calculations, the local density of states above the Fermi level is the highest on the adatoms as compared to the rest atoms and first- and second-layer atoms, in agreement with the results in Refs. 1 and 3. We therefore propose that strongest screening of adatoms is due to this unoccupied band, which can move downward below the Fermi

level in the final state. For the rest atoms, the Δ_{SCLS} is positive. It is 0.077 [0.119] eV for the R_R [R_T] in the T_4 structure, and 0.023 [0.001] eV in the H_3 structure, respectively. Therefore, the screening of rest atoms has a specific character and, for this reason, we will not consider the rest atoms below.

A closer inspection of Δ_{SCLS} values in Fig. 6 indicates that the efficiency of screening differs substantially in the two atomic structures. For the H_3, the absolute value of Δ_{SCLS} decreases monotonously from 0.441 to 0.455 for the topmost atoms (i.e., the adatoms) to 0.064–0.104 for the third-layer atoms. Such behavior is predicted for semiconductor surfaces (see, e.g., Ref. 27). In contrast, the absolute values of Δ_{SCLS} for the adatoms, the first-layer atoms, the 2A atom, and the 3A atom in the T_4 structure are very similar (0.223–0.234, 0.162–0.182, 0.185, and 0.212 eV, respectively). For the other second- and third-layer atoms in this structure, the absolute value of Δ_{SCLS} is noticeably smaller (0.025–0.066 eV), and the screening is weak. Thus, the significant screening in the T_4 structure can occur locally in the vicinity of the adatoms, and it can effectively penetrate beneath the surface, with the Δ_{SCLS} being approximately the same for the adatoms, the first-layer atoms, the 2_A atom, and the 3_A atom. Taking into account

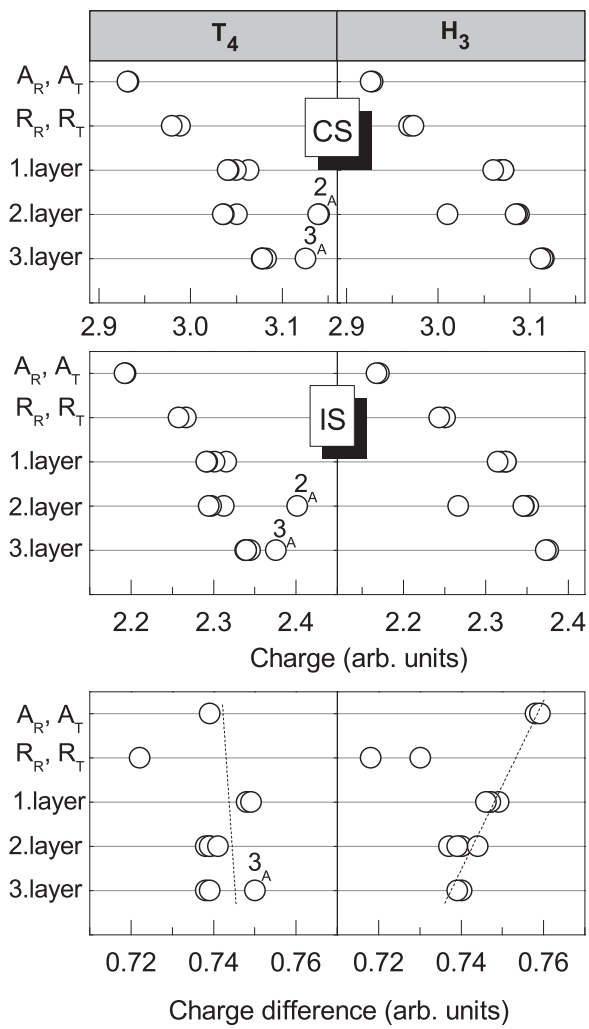

FIG. 7. Comparison of on-site charges in the initial state and complete screening models, and charge differences for the T_4 and H_3 structures.

that the 2_A atom is located just below the adatom and the 3_A atom is located just below the 2_A atom, such penetration infers a vertical screening channel which is due to the specific atomic geometry in the case of the adatoms at T_4 sites. It is worth mentioning that in the H_3 structure, the adatom is located above a fourth-layer atom, and the screening effects reveal different trends in such an atomic geometry. Thus, the screening and geometric effects correlate in the T_4 and H_3 structures. Note that the presence of specific 2_A and 3_A atoms in the distorted second and third layers of the T_4 structure leads to additional vibrational (phonon) modes on Ge(111)$c(2\times 8)$ (Ref. 3), which seems to correlate with the finding of vertical screening channel in this study.

In order to gain additional information about the screening in the T_4 and H_3 structures, we have calculated on-site charges of different atoms in the initial state and the complete screening state (Fig. 7). The differences between these charges are also shown in the bottom panel of Fig. 7. As seen, the charge difference is smallest for the rest atoms, in full agreement with the Δ_{SCLS} results in Fig. 6. Furthermore, the trends in Figs. 6 and 7 reasonably correlate to each other for both atomic structures. In particular, the screening charge is largest for the adatoms and decreases for deeper atoms in the H_3 structure. A different tendency is found for the T_4 structure, where the screening charge is roughly unchanged along the vertical screening channel. Thus, the Δ_{SCLS} data is supported well by the on-site charge calculation.

IV. CONCLUSIONS

The $3d$ photoemission line shape and SCLSs have been reinvestigated on the Ge(111)$c(2\times 8)$ reconstruction both experimentally and theoretically. It is found that the $3d$ spectra can be deconvoluted by using five components which are B, S_1, S_2, S_3, and S_4. The SCLSs of S_1, S_2, S_3, and S_4 are -0.290, -0.755, 0.150, and -0.125 eV relative to B, respectively. The DFT calculations clarify the origin of these components in detail. The S_1 and S_4 originate from the first- and second-layer atoms in the T_4 structure. The S_2 is caused by the rest atoms, while the S_3 is due to the adatoms and the 3_A atoms. In addition, the DFT calculations support the T_4 site for the adatoms on Ge(111)$c(2\times 8)$ and demonstrate that this structure is in a better agreement with the $3d$ photoemission line shape than the structure where the adatoms reside at H_3. It is found that the initial state theory can reproduce the measured SCLS adequately, while such shifts are overestimated within the complete screening approach. Finally, the interplay between the screening effects and the atomic structure of Ge(111)$c(2\times 8)$ is discussed.

ACKNOWLEDGMENTS

We are grateful to H. Ollila and the MAX-lab staff for technical assistance. The financial supports by the Academy of Finland (Grants No. 122743 and No. 122355), Finnish Academy of Science and Letters, the Carl Tryggers Foundation (M.P.J.P.), the Emil Aaltonen Foundation (M.P.J.P.), and the European Community's Seventh Framework Programme (FP7/2007-2013) under Grant No. 226716 are kindly acknowledged.

*Corresponding author: m.kuzmin@mail.ioffe.ru.

[1]N. Takeuchi, A. Selloni, and E. Tosatti, Phys. Rev. Lett. **69**, 648 (1992).
[2]N. Takeuchi, A. Selloni, and E. Tosatti, Phys. Rev. B **51**, 844 (1995).
[3]I. Razado-Colambo, J. Selloni, H. M. Zhang, G. V. Hansson, and R. I. G. Uhrberg, Phys. Rev. B **79**, 205410 (2009).
[4]S. B. DiCenzo, P. A. Bennett, D. Tribula, P. Thiry, G. K. Wertheim, and J. E. Rowe, Phys. Rev. B **31**, 2330 (1985).
[5]R. D. Bringans, M. A. Olmstead, R. J. G. Uhrberg, and R. Z. Bachrach, Phys. Rev. B **36**, 9569 (1987).
[6]J. Aarts, A.-J. Hoeven, and P. K. Larsen, Phys. Rev. B **38**, 3925 (1988).
[7]K. Hricovini, G. Le Lay, M. Abraham, and J. E. Bonnet, Phys. Rev. B **41**, 1258 (1990).
[8]L. Patthey, E. L. Bullock, and K. Hricovini, Surf. Sci. **269/270**, 28 (1992).
[9]D. H. Rich, T. Miller, and T.-C. Chiang, Phys. Rev. Lett. **60**, 357 (1988).
[10]A. L. Wachs, T. Miller, A. P. Shapiro, and T.-C. Chiang, Phys. Rev. B **35**, 5514 (1987).
[11]M. T. Sieger, J. M. Roesler, D.-S. Lin, T. Miller, and T.-C. Chiang, Phys. Rev. Lett. **73**, 3117 (1994).
[12]M. Göthelid, T. M. Grehk, M. Hammar, U. O. Karlsson, and S. A. Flodström, Phys. Rev. B **48**, 2012 (1993).
[13]A. Santoni, V. R. Dhanak, A. Goldoni, M. Sancrotti, and S. Modesti, Europhys. Lett. **34**, 275 (1996).
[14]A. Goldoni, A. Santoni, M. Sancrotti, V. R. Dhanak, and S. Modesti, Surf. Sci. **382**, 336 (1997).
[15]G. Kresse and J. Hafner, Phys. Rev. B **47**, 558 (1993); **49**, 14251 (1994); G. Kresse and J. Furthmüller, Comput. Mat. Sci. **6**, 15 (1996); G. Kresse and J. Hafner, Phys. Rev. B **54**, 11169 (1996).
[16]P. E. Blöchl, Phys. Rev. B **50**, 17953 (1994); G. Kresse and D. Joubert, *ibid.* **59**, 1758 (1999).
[17]D. M. Ceperley and B. J. Alder, Phys. Rev. Lett. **45**, 566 (1980).
[18]J. P. Perdew and A. Zunger, Phys. Rev. B **23**, 5048 (1981).
[19]G. Kresse and J. Furthmüller, *Vienna Ab Initio Simulation Package, Users Guide* (The University of Vienna, Vienna, 2007).
[20]L. Köhler and G. Kresse, Phys. Rev. B **70**, 165405 (2004).
[21]M. Göthelid, M. Hammar, M. Björkqvist, U. O. Karlsson, S. A. Flodström, C. Wigren, G. LeLay, Phys. Rev. B **50**, 4470 (1994).
[22]M. Göthelid, M. Hammar, U. O. Karlsson, C. Wigren, G. LeLay, Phys. Rev. B **52**, 14104 (1995).
[23]M. Göthelid, G. LeLay, C. Wigren, M. Björkqvist, U. O. Karlsson, Surf. Sci. **371**, 264 (1997).
[24]P. E. J. Eriksson and R. I. Uhrberg, Phys. Rev. B **81**, 125443 (2010).
[25]M. Kuzmin, P. Laukkanen, R. E. Perälä, M. Ahola-Tuomi, and I. J. Väyrynen, Surf. Sci. **601**, 837 (2007).
[26]M. Kuzmin, P. Laukkanen, R. E. Perälä, M. Ahola-Tuomi, and I. J. Väyrynen, J. Electron Spectrosc. **159**, 24 (2007).
[27]E. Pehlke and M. Scheffler, Phys. Rev. Lett. **71**, 2338 (1993).